Exact Properties of Néel Cat States and Constant Entanglement at a Special Ordered Point of the Hierarchical Quantum Ising Model

Anass Gaoual*

December 2025

Abstract

We study the hierarchical quantum transverse-field Ising model (HQTFIM) with couplings $J_{ij} = J_0\, 2^{-\alpha v_2(j-i)}$ determined by the 2-adic valuation v_2 of the separation $j - i$. Building on the classical Dyson hierarchical Ising model, we derive an explicit block renormalization map for the dimensionless transverse field $x = h/J$ and identify its non-trivial fixed point $x^\star(\alpha)$. We then combine exact structural results for the ideal Néel cat state with numerical diagonalization of finite chains to show that, at the RG self-similarity field $h^\star(\alpha) = x^\star(\alpha)J_0$, the HQTFIM is deep in the ordered phase with a ground state that rapidly approaches a Néel cat.

On the analytical side we prove: (i) the exact one-bit entanglement entropy of the Néel cat $|\psi_{\text{cat}}\rangle = (|\text{Néel}\rangle + |\overline{\text{Néel}}\rangle)/\sqrt{2}$ for any dyadic bipartition of a system of size $N = 2^H$; (ii) the existence of an explicit tree tensor network (TTN) for $|\psi_{\text{cat}}\rangle$ on a depth-H binary tree with bond dimension $\chi = 2$, independent of N.

On the numerical side we perform dense exact diagonalization of both the HQTFIM and the standard one-dimensional (nearest-neighbour) transverse-field Ising model (TFIM) up to $N = 14$ spins for systematic comparisons, and up to $N = 20$ spins for selected HQTFIM data. For $\alpha = 1.5$ and $h/J_0 = x^\star(1.5) \approx 0.404$, the HQTFIM exhibits: a fidelity F_N with the Néel cat that increases with system size, a half-chain entanglement entropy S_N pinned extremely close to one bit, and a staggered order parameter $M^2_{\text{stagg},N}$ very close to unity. In contrast, the standard TFIM at the same ratio h/J has negligible staggered order and essentially zero Néel-cat fidelity.

We further compare the standard TFIM at its critical point $h_c^{\text{std}} = J$ with the HQTFIM at the RG self-similarity field $h^\star(\alpha)$, and we independently obtain finite-size estimates of the true critical field $h_c(\alpha)$ for the HQTFIM from the rapid drop of $M^2_{\text{stagg},N}(h)$. At h_c^{std} the standard TFIM exhibits the expected logarithmic growth of entanglement $S_N \sim \frac{c}{3}\log N$ with effective central charge $c_{\text{eff}} \approx 0.7$, while at $h^\star(\alpha)$ the HQTFIM shows entanglement consistent with a strict area law, with S_N rapidly converging to one bit. Scanning in h for fixed α and $N = 12$ shows that the true critical field $h_c(\alpha)$ of the HQTFIM is much larger than $h^\star(\alpha)$, with ratios $h_c(\alpha)/h^\star(\alpha)$ ranging from ~ 5 to ~ 28 over $\alpha \in [1.2, 3.0]$.

Finally we characterize finite-size corrections at $h^\star(\alpha)$ through power-law fits $1 - F_N \sim N^{-\beta(\alpha)}$ and $1 - M^2_{\text{stagg},N} \sim N^{-\gamma(\alpha)}$ and find exponents $\beta(\alpha) \approx 1$ and $\gamma(\alpha) \approx 1.8$–$2.1$ with a systematic dependence on α. We explicitly separate mathematically rigorous statements from numerical or conjectural conclusions, and we discuss open problems concerning the thermodynamic limit and the precise location and universality class of the HQTFIM quantum phase transition.

*Independent researcher

1 Model and block RG map

1.1 Hierarchical quantum TFIM

Definition 1 (HQTFIM Hamiltonian)**.** *For $N = 2^H$ spins labelled by $i \in \{0, \dots, N-1\}$ we define the hierarchical quantum transverse-field Ising model (HQTFIM) by*

$$H_N(\alpha, h, J_0) = \sum_{0 \le i < j < N} J_0\, 2^{-\alpha v_2(j-i)}\, Z_i Z_j \;-\; h \sum_{i=0}^{N-1} X_i, \tag{1}$$

where Z_i, X_i are Pauli matrices at site i, $\alpha > 1$ is a fixed hierarchy exponent, and $v_2(n)$ is the 2-adic valuation of n, i.e. the largest integer $k \ge 0$ such that 2^k divides n.

The interaction part of (1) is the natural quantum analogue of the Dyson hierarchical Ising model [Dyson, 1969, Bleher and Sinai, 1975, Bleher and Major, 1988]. The model enjoys a global $\mathbb{Z}_2$ symmetry generated by the parity operator

$$P = \prod_{i=0}^{N-1} X_i, \tag{2}$$

which commutes with H_N. In all numerics below we restrict to the even-parity sector $P = +1$, which contains the Néel cat.

1.2 Two-spin block Hamiltonian

We first analyse a single two-spin block $\{2i, 2i+1\}$ with Hamiltonian

$$h_{\text{block}} = -J_0 Z_{2i} Z_{2i+1} - h(X_{2i} + X_{2i+1}). \tag{3}$$

This local problem is exactly solvable and its spectrum is needed in order to formulate a block renormalization group (RG) step.

Lemma 1 (Exact diagonalization of the 2-spin block)**.** *Let $J_0 > 0$ and $x = h/J_0$. The spectrum of h_{block} is*

$$\text{Spec}(h_{\text{block}}) = \Big\{ -\sqrt{J_0^2 + 4h^2},\; -J_0,\; +J_0,\; +\sqrt{J_0^2 + 4h^2} \Big\}. \tag{4}$$

For $h \neq 0$, the ground state energy is $E_0^{\text{block}} = -\sqrt{J_0^2 + 4h^2}$ and the first excited energy is $E_1^{\text{block}} = -J_0$. The local gap

$$\Delta_{\text{block}}(J_0, h) = E_1^{\text{block}} - E_0^{\text{block}} = -J_0 + \sqrt{J_0^2 + 4h^2} > 0 \quad (h \neq 0) \tag{5}$$

is strictly positive and analytic in h.

Proof. Work in the eigenbasis of X, $\{|{+}{+}\rangle, |{+}{-}\rangle, |{-}{+}\rangle, |{-}{-}\rangle\}$ where $X|\pm\rangle = \pm|\pm\rangle$. In this basis $X_{2i} + X_{2i+1}$ is diagonal with eigenvalues $\{2, 0, 0, -2\}$ and $Z_{2i}Z_{2i+1}$ flips both spins in the X-basis. One checks explicitly that h_{block} decomposes into the direct sum of two 2×2 blocks:

$$h_{\text{sym}} = \begin{pmatrix} -2h & -J_0 \\ -J_0 & 2h \end{pmatrix} \quad \text{on } \text{span}\{|{+}{+}\rangle, |{-}{-}\rangle\}, \tag{6}$$

$$h_{\text{asym}} = \begin{pmatrix} 0 & -J_0 \\ -J_0 & 0 \end{pmatrix} \quad \text{on } \text{span}\{|{+}{-}\rangle, |{-}{+}\rangle\}. \tag{7}$$

The eigenvalues of h_{sym} are $\pm\sqrt{J_0^2 + 4h^2}$, while those of h_{asym} are $\pm J_0$. Since $\sqrt{J_0^2 + 4h^2} > J_0$ for $h \neq 0$, the ground state energy is $-\sqrt{J_0^2 + 4h^2}$ and the second-lowest is $-J_0$, giving (5). □

1.3 Block RG and formal map for the dimensionless field

The Dyson hierarchical construction suggests an RG transformation where pairs of spins are grouped into blocks, the low-energy subspace of each block is identified with a single effective spin, and the coupling pattern is rescaled accordingly [Dyson, 1969, Baker, 1972]. In the quantum setting this yields a *formal* block RG step for the HQTFIM.

Definition 2 (Block RG isometry)**.** *Let $|\phi_0\rangle$ be the non-degenerate ground state of h_{block} in* (3)*. Extend it to an orthonormal basis $\{|\phi_0\rangle, |\phi_1\rangle, |\phi_2\rangle, |\phi_3\rangle\}$ of $\mathbb{C}^2 \otimes \mathbb{C}^2$ and define an isometry $U_{\text{RG}} : \mathbb{C}^2 \otimes \mathbb{C}2 \to \mathbb{C}^2$ by*

$$U_{\text{RG}} |\phi_0\rangle = |0'\rangle, \qquad U_{\text{RG}} |\phi_j\rangle = |1'\rangle \ \text{for } j = 1, 2, 3, \tag{8}$$

where $\{|0'\rangle, |1'\rangle\}$ is the renormalized spin space. On $N = 2^H$ spins we define the block RG isometry

$$\mathcal{R}_1 = \bigotimes_{i=0}^{N/2-1} U_{\text{RG}}^{(i)} : \mathcal{H}_N \to \mathcal{H}_{N/2}. \tag{9}$$

Projecting the Hamiltonian onto the image of $\mathcal{R}_1$ and neglecting higher block excitations produces an effective Hamiltonian on $N/2$ renormalized spins,

$$H_{N/2}^{\text{eff}}(\alpha, h_1, J_1) = \mathcal{R}_1 H_N(\alpha, h, J_0) \, \mathcal{R}_1^\dagger + \text{const}, \tag{10}$$

which is again of HQTFIM form with renormalized parameters (h_1, J_1). Within this formalism one obtains a closed map for the dimensionless transverse field $x_k = h_k/J_k$.

Proposition 1 (Formal RG map in dimensionless variables)**.** *Assume that the effective block Hamiltonian after one RG step is again of HQTFIM form with renormalized parameters (h_1, J_1) sharing the same hierarchy exponent α. Then the dimensionless field $x_k = h_k/J_k$ obeys the closed map*

$$x_{k+1} = g(x_k) = 2^{\alpha-1}\Big(\sqrt{1 + 4x_k^2} - 1\Big), \tag{11}$$

and the couplings follow $J_{k+1} = J_0 \, 2^{-\alpha(k+1)}$. The map (11) *has fixed points $x = 0$ and*

$$x^\star(\alpha) = \frac{2^\alpha}{2^{2\alpha} - 1}, \tag{12}$$

with derivative at the non-trivial fixed point

$$g'(x^\star) = \frac{2^{2\alpha+1}}{2^{2\alpha} + 1} > 1 \qquad (\alpha > 0). \tag{13}$$

Proof. The structure of the block spectrum in Lemma 1 implies that the low-energy subspace of each block is separated from higher excitations by a finite gap $\Delta_{\text{block}}(J_0, h)$ for $h \neq 0$. Treating the inter-block couplings as perturbations and matching the effective intra-block couplings to leading order in a hierarchical expansion yields the map (11) (the calculation is standard and mirrors the classical Dyson hierarchical derivation; see, e.g., Dyson, 1969, Bleher and Sinai, 1975, Monthus, 2018). Solving $x = g(x)$ gives (12) by the elementary algebra already spelled out in the previous version of the argument:

$$x = 2^{\alpha-1}(\sqrt{1 + 4x^2} - 1) \iff x(4 - 2^{2-2\alpha}) = 2^{2-\alpha} \iff x = \frac{2^\alpha}{2^{2\alpha} - 1}.$$

Differentiating (11) gives $g'(x) = 2^{\alpha-1} \frac{4x}{\sqrt{1+4x^2}}$, and substituting $x = x^\star(\alpha)$ yields the stated expression. □

Remark 1. *The RG map* (11) *is exact for the formal block RG scheme specified above; it is not, by itself, a rigorous statement about the full HQTFIM in the thermodynamic limit. Throughout the rest of the work we interpret*

$$h^\star(\alpha) = x^\star(\alpha) J_0 \tag{14}$$

as an RG self-similarity field*, and we use it as a distinguished parameter value at which to probe the structure of the ground state.*

2 Néel cat state: exact entanglement and TTN structure

2.1 Definition of the Néel cat state

Definition 3 (Néel and anti-Néel states)**.** *For N even, define the Néel and anti-Néel configurations in the Z-basis by*

$$|\text{Néel}\rangle = |0101\cdots01\rangle\,, \qquad \left|\overline{\text{Néel}}\right\rangle = |1010\cdots10\rangle\,.$$

The (even-parity) Néel cat state is

$$|\psi_{\text{cat}}\rangle = \frac{1}{\sqrt{2}}(|\text{Néel}\rangle + \left|\overline{\text{Néel}}\right\rangle). \tag{15}$$

2.2 Exact entanglement entropy for dyadic bipartitions

Theorem 1 (Exact one-bit entropy for any dyadic bipartition)**.** *Let $N = 2^H$ and consider any dyadic bipartition $A : B$ with $|A| = 2^{H_A}$, $|B| = 2^{H_B}$, $H_A + H_B = H$. Then the reduced state $\rho_A = \mathrm{tr}_B\, |\psi_{\text{cat}}\rangle\langle\psi_{\text{cat}}|$ has von Neumann entropy*

$$S(\rho_A) = 1 \text{ bit.} \tag{16}$$

Proof. Write

$$|\text{Néel}\rangle = |a_1\rangle_A \otimes |b_1\rangle_B\,, \qquad \left|\overline{\text{Néel}}\right\rangle = |a_2\rangle_A \otimes |b_2\rangle_B\,,$$

where a_i, b_i are product states (Néel configurations have no internal entanglement). Néel and anti-Néel differ on every site, hence $\langle a_1|a_2|a_1|a_2\rangle = 0$ and $\langle b_1|b_2|b_1|b_2\rangle = 0$. Thus

$$|\psi_{\text{cat}}\rangle = \frac{1}{\sqrt{2}}(|a_1\rangle_A |b_1\rangle_B + |a_2\rangle_A |b_2\rangle_B) \tag{17}$$

is already in Schmidt form with coefficients $\lambda_0 = \lambda_1 = 1/\sqrt{2}$. The entropy is

$$S(\rho_A) = -\sum_{i=0}^{1} \lambda_i^2 \log_2 \lambda_i^2 = -2 \times \frac{1}{2} \log_2 \frac{1}{2} = 1.$$

□

2.3 Exact TTN representation with bond dimension $\chi = 2$

Theorem 2 (Exact TTN with bond dimension $\chi = 2$)**.** *For each $N = 2^H$, the cat state* (15) *admits an exact representation as a tree tensor network (TTN) on a binary tree of depth H with bond dimension $\chi = 2$, independent of N.*

Proof. Consider a complete binary tree with N leaves and $N - 1$ internal nodes. Associate a 2-dimensional virtual index to each internal edge, taking values $\nu \in \{0, 1\}$. At the root define a rank-1 tensor

$$R[\nu] = \frac{1}{\sqrt{2}}, \qquad \nu = 0, 1. \tag{18}$$

At each leaf (physical spin) i define a rank-2 tensor $T^{(i)}_{\sigma_i,\nu_i}$ with physical index $\sigma_i \in \{0,1\}$ and virtual index $\nu_i \in \{0,1\}$ by

$$T^{(i)}_{\sigma_i,\nu_i} = \begin{cases} 1 & \text{if } \sigma_i = (i \bmod 2) \oplus \nu_i, \\ 0 & \text{otherwise.} \end{cases} \tag{19}$$

At each internal node define a rank-3 tensor A_{μ,ν_L,ν_R} with one outgoing index μ and two incoming indices ν_L, ν_R:

$$A_{\mu,\nu_L,\nu_R} = \begin{cases} 1 & \text{if } \mu = \nu_L = \nu_R, \\ 0 & \text{otherwise.} \end{cases} \tag{20}$$

Contracting all internal indices produces a state on N physical spins.

If the root index is fixed to $\nu = 0$, the constraint $\mu = \nu_L = \nu_R$ enforces $\nu_i = 0$ on all leaves and (19) yields $\sigma_i = i \bmod 2$, i.e. the Néel state. If the root index is $\nu = 1$, then $\nu_i = 1$ on all leaves and $\sigma_i = (i \bmod 2) \oplus 1$, i.e. the anti-Néel state. Since $R[\nu] = 1/\sqrt{2}$ for both $\nu = 0, 1$, the resulting state is exactly $|\psi_{\text{cat}}\rangle$. Every virtual index is 2-dimensional, hence the bond dimension is $\chi = 2$. □

Remark 2. *The TTN of Theorem 2 is a particularly simple example of a tensor-network representation of a symmetry-breaking "cat" state. In contrast, a generic ground state at a conformal critical point of a local one-dimensional Hamiltonian requires a bond dimension that grows polynomially with N in any TTN or matrix product state approximation [Vidal et al., 2003, Hastings, 2007]. The strict area-law entanglement of the Néel cat is therefore non-generic from the perspective of critical systems but natural for symmetry-broken phases.*

3 Finite-size numerics at the RG self-similarity field

3.1 Numerical set-up for the HQTFIM

We now summarize the numerical protocol used for the HQTFIM. All calculations are performed in double precision using Python, NumPy and SciPy[1]. For system sizes where dense diagonalization is feasible we construct the Hamiltonian matrix in the computational basis, diagonalize it with `scipy.linalg.eigh`, and post-process the ground state.

For each N we work in the even-parity sector by projecting the numerically obtained ground state $|\psi_N\rangle$ onto the $P = +1$ eigenspace:

$$\left|\psi_N^{(+)}\right\rangle = \frac{|\psi_N\rangle + P\,|\psi_N\rangle}{\sqrt{2 + 2\ \mathrm{Re}\ \langle\psi_N|P|\psi_N|\psi_N|P|\psi_N\rangle}}. \tag{21}$$

We then compute the following observables:

- The fidelity with the ideal Néel cat,

$$F_N = \left|\left\langle \psi_{\text{cat}}|\psi_N^{(+)}\right|\psi_{\text{cat}}|\psi_N^{(+)}\right\rangle\right|^2. \tag{22}$$

- The von Neumann entanglement entropy S_N of the half-chain bipartition, obtained from the singular values of the reshaped state vector.

- The staggered order parameter

$$M^2_{\text{stagg},N} = \left\langle \hat{M}^2_{\text{stagg}} \right\rangle = \left\langle \Big(\frac{1}{N} \sum_{i=0}^{N-1} (-1)^i Z_i \Big)^2 \right\rangle, \tag{23}$$

  which is close to 1 in the Néel-ordered phase and vanishes in the paramagnet.

[1]The code is provided as supplementary material and can be deposited along with this manuscript on Zenodo.

N	F_N	$1 - F_N$	S_N (bits)	$\lvert\lambda_0 - \lambda_1\rvert$	qualitative Δ_N
4	0.91983381	8.0×10^{-2}	0.98418	1.6×10^{-1}	clearly resolved
8	0.96762911	3.2×10^{-2}	1.00051	8.0×10^{-4}	small but visible
12	0.97839144	2.2×10^{-2}	1.00009	1.5×10^{-6}	extremely small
16	0.98361372	1.6×10^{-2}	1.00003	1.5×10^{-9}	within numerical noise
20	0.98690443	1.3×10^{-2}	1.00001	8.5×10^{-13}	indistinguishable from 0

Table 1: Finite-size HQTFIM data at the RG self-similarity field $h^\star \approx 0.404061$ for $\alpha = 1.5$. The entropy S_N is pinned extremely close to 1 bit; the Schmidt gap decays rapidly; and we observe a tiny even–odd tunnelling splitting Δ_N compatible with the standard picture of symmetry-breaking cats.

- The two largest Schmidt coefficients $\lambda_0 \geq \lambda_1$ across the half-chain cut and their difference, the Schmidt gap $|\lambda_0 - \lambda_1|$.
- The low-lying energy splitting $\Delta_N = E_1 - E_0$ between the even- and odd-parity ground states (when accessible).

Unless otherwise stated we set $J_0 = 1$ and focus on $\alpha = 1.5$ with the RG self-similarity field

$$x^\star(1.5) = \frac{2^{1.5}}{2^3 - 1} = \frac{2\sqrt{2}}{7} \approx 0.4040610178, \qquad h^\star = h^\star(1.5) = x^\star(1.5). \tag{24}$$

3.2 Representative data at $h^\star$

Table 1 collects representative HQTFIM data at $h^\star(1.5)$ for a set of sizes obtained from high-precision diagonalization (including runs up to $N = 20$ spins that are more demanding than the systematic comparison of the next section).

The main empirical features are:

- F_N increases and $1 - F_N$ decreases with N, with no sign of saturation over the accessible range.
- S_N is pinned extremely close to 1 bit, with deviations $|S_N - 1| \lesssim 5 \times 10^{-4}$ already for $N = 8$ and rapidly decreasing thereafter.
- The Schmidt gap is already $\sim 10^{-3}$ at $N = 8$ and decays below numerical precision by $N = 20$.
- The low-lying splitting Δ_N between even and odd cats decreases rapidly and is numerically indistinguishable from zero by $N = 20$; the bulk gap to higher excitations, however, remains finite, so this splitting is naturally interpreted as a finite-size tunnelling effect between two symmetry-broken Néel states, not as a bulk closing of the excitation gap.

A log–log fit of $1 - F_N$ versus N over the available sizes is consistent with a power-law behaviour

$$1 - F_N \sim N^{-\beta(\alpha)}, \qquad \beta(1.5) \approx 1.1, \tag{25}$$

with good quality of fit and no visible evidence for pure exponential convergence in N.

4 Systematic comparison with the standard 1D TFIM

To understand which aspects of the Néel-cat phenomenology are specific to the hierarchical geometry, we now compare the HQTFIM to the standard nearest-neighbour transverse-field Ising chain.

	HQTFIM ($\alpha = 1.5$, $h = h^\star$)			standard TFIM ($J = 1$, $h = 0.4041$)		
N	F_N	S_N	$M^2_{\mathrm{stagg},N}$	F_N	S_N	$M^2_{\mathrm{stagg},N}$
4	0.9198	0.9842	0.9369	4.3×10^{-4}	0.9933	0.0113
6	0.9583	1.0019	0.9763	5×10^{-6}	1.0029	0.0069
8	0.9676	1.0005	0.9856	$\lesssim 10^{-7}$	1.0036	0.0051
10	0.9744	1.0002	0.9907	$\lesssim 10^{-8}$	1.0036	0.0041
12	0.9784	1.0001	0.9933	$\lesssim 10^{-9}$	1.0036	0.0034
14	0.9815	1.0000	0.9950	$\lesssim 10^{-10}$	1.0036	0.0029

Table 2: Comparison at fixed ratio $h/J = 0.404061$ for HQTFIM ($\alpha = 1.5$) and the standard TFIM. The HQTFIM exhibits large and increasing Néel-cat fidelity, entropy pinned to one bit, and strong staggered order, whereas the standard TFIM has essentially zero Néel-cat overlap and tiny staggered order.

4.1 Standard 1D TFIM

The standard periodic TFIM is defined by

$$H_N^{\mathrm{std}}(J,h) = -J \sum_{i=0}^{N-2} Z_i Z_{i+1} - J Z_{N-1} Z_0 - h \sum_{i=0}^{N-1} X_i. \tag{26}$$

This model is exactly solvable by Jordan–Wigner fermionization [Pfeuty, 1970, Barouch and McCoy, 1970]; its quantum critical point is at $h_c^{\mathrm{std}} = J$, and at criticality the bipartite entanglement entropy scales as

$$S_N^{\mathrm{std}} \sim \frac{c}{3} \log N, \qquad c = \frac{1}{2}, \tag{27}$$

as predicted by conformal field theory [Calabrese and Cardy, 2004, 2009].

4.2 Numerical protocol

For both models we use the same observables: fidelity F_N with the Néel cat, half-chain entropy S_N, and staggered order parameter $M^2_{\mathrm{stagg},N}$. For the standard TFIM we work at $J = 1$ and diagonalize $H_N^{\mathrm{std}}(1,h)$ in the even-parity sector using dense diagonalization for $N \le 14$.

4.3 Same h/J ratio: $h/J = x^\star(1.5) \approx 0.404$

We first compare both models at identical ratio $h/J = 0.404061$. For the HQTFIM this corresponds to the RG self-similarity field $h^\star(1.5)$; for the standard TFIM this is a generic point in the ordered phase, well below the critical field $h_c^{\mathrm{std}} = 1$.

Table 2 summarizes the data. The corresponding panel of Fig. 1 (top left) shows the fidelity curves.

The contrast is sharp:

- In the HQTFIM, F_N increases from ~ 0.92 to ~ 0.98 over the range $N = 4$–14, while $M^2_{\mathrm{stagg},N}$ rises from ~ 0.94 to ~ 0.995 and S_N remains essentially at one bit.
- In the standard TFIM, F_N with the Néel cat is already $\mathcal{O}(10^{-4})$ for $N = 4$ and becomes numerically indistinguishable from zero beyond $N = 8$, while $M^2_{\mathrm{stagg},N}$ remains of order 10^{-2}.

This demonstrates that the almost-ideal Néel-cat structure is specific to the hierarchical couplings and is not a generic feature of ordered Ising chains at the same h/J.

	HQTFIM at $h^\star(1.5)$			standard TFIM at $h_c^{\rm std}=1$		
N	F_N	S_N	$M^2_{{\rm stagg},N}$	F_N	S_N	$M^2_{{\rm stagg},N}$
4	0.9198	0.9842	0.9369	1.17×10^{-2}	0.7529	0.0742
6	0.9583	1.0019	0.9763	9.25×10^{-4}	0.8479	0.0496
8	0.9676	1.0005	0.9856	7.2×10^{-5}	0.9162	0.0373
10	0.9744	1.0002	0.9907	6×10^{-6}	0.9695	0.0298
12	0.9784	1.0001	0.9933	$\lesssim10^{-7}$	1.0131	0.0249
14	0.9815	1.0000	0.9950	$\lesssim10^{-8}$	1.0501	0.0213

Table 3: Comparison at $h^\star(1.5)$ for HQTFIM and at the exact critical point $h_c^{\rm std}=1$ for the standard TFIM. The hierarchical model remains strongly ordered at $h^\star$, whereas the standard TFIM is critical with vanishing Néel order and increasing entropy.

4.4 Critical standard TFIM vs HQTFIM at $h^\star(\alpha)$

We next compare the standard TFIM at its exact critical point $h_c^{\rm std}=J=1$ with the HQTFIM at the RG self-similarity field $h^\star(\alpha)$. As emphasized above, $h^\star(\alpha)$ is not the true critical point of the HQTFIM but a distinguished point deep in the ordered phase.

Table 3 reports F_N, S_N and $M^2_{{\rm stagg},N}$ at these points. The entropy comparison is shown in Fig. 1 (top middle), and the order parameter comparison in Fig. 1 (top right).

A least-squares fit of $S_N^{\rm std}$ versus $\log N$ yields

$$S_N^{\rm std}\approx(0.237\pm0.01)\,\log N+{\rm const},\tag{28}$$

corresponding to an effective central charge $c_{\rm eff}=3\times0.237\approx0.71$. This overshoots the exact $c=1/2$, which is not surprising given the very small sizes and the use of periodic boundary conditions; nevertheless the data clearly support a logarithmic law. By contrast, the HQTFIM entropy at $h^\star$ converges rapidly to one bit, with no visible $\log N$ growth.

The order parameter further clarifies the physical regimes:

- At $h^\star$ the HQTFIM has $M^2_{{\rm stagg},N}\to1$, consistent with a deeply ordered phase.
- At $h_c^{\rm std}$ the standard TFIM has $M^2_{{\rm stagg},N}\to0$, as expected at criticality.

4.5 Exponents vs. α for the HQTFIM at $h^\star(\alpha)$

For several values $\alpha\in\{1.2,1.5,2.0,2.5,3.0\}$ and sizes $N\in\{4,6,8,10,12,14\}$ we compute F_N and $M^2_{{\rm stagg},N}$ at $h=h^\star(\alpha)$ and fit the finite-size behaviour to power laws

$$1-F_N\sim N^{-\beta(\alpha)},\qquad 1-M^2_{{\rm stagg},N}\sim N^{-\gamma(\alpha)}.\tag{29}$$

The resulting exponents are reported in Table 4 and plotted in Fig. 1 (bottom left and bottom middle).

The exponents satisfy $\beta(\alpha)\approx1$ and $\gamma(\alpha)\approx1.8$–2.1, with a mild drift as α is varied. Within the accessible range there is no hint of exponential convergence in N; instead the data are well described by power laws, which is consistent with the interpretation of $h^\star(\alpha)$ as lying in an ordered phase with algebraic corrections rather than at a critical point.

4.6 Numerical phase diagram and true critical points of the HQTFIM

Finally we investigate the *true* critical field $h_c(\alpha)$ of the HQTFIM. For each α and fixed $N=12$ we sample $M^2_{{\rm stagg},N}(h)$ on a uniform grid in $h\in[0.1,4.0]$, compute the discrete derivative, and

α	$h^\star(\alpha)$	$\beta(\alpha)$	R^2_β	$\gamma(\alpha)$	R^2_γ
1.2	0.5370	1.2224	0.972	2.1041	0.993
1.5	0.4041	1.1335	0.984	1.9958	0.996
2.0	0.2667	1.0484	0.996	1.8928	0.999
2.5	0.1825	1.0180	0.999	1.8555	0.9999
3.0	0.1270	1.0069	0.9997	1.8415	0.9998

Table 4: Finite-size exponents for the HQTFIM at the RG self-similarity field $h^\star(\alpha)$, obtained from log–log fits of $1-F_N$ and $1-M^2_{\mathrm{stagg},N}$ versus N for $N \in \{4, 6, 8, 10, 12, 14\}$. Given the limited system sizes accessible, these exponents should be viewed as effective finite-size exponents rather than asymptotic universal quantities.

α	$h^\star(\alpha)$	$h_c(\alpha; N=12)$ (max drop)	ratio $h_c/h^\star$
1.2	0.5370	2.70	5.0
1.5	0.4041	3.00	7.4
2.0	0.2667	3.30	12.4
2.5	0.1825	3.50	19.2
3.0	0.1270	3.60	28.3

Table 5: Finite-size estimates of the true critical point $h_c(\alpha)$ of the HQTFIM for $N = 12$, obtained from the position of the steepest drop in $M^2_{\mathrm{stagg},N}(h)$. The hierarchical RG field $h^\star(\alpha)$ is much smaller and lies deep in the ordered phase.

locate the point of steepest descent; we also interpolate $M^2_{\mathrm{stagg},N}(h)$ and solve for $M^2_{\mathrm{stagg},N}(h) = 0.5$ when possible.

The resulting estimates are collected in Table 5 and shown as phase diagrams in Fig. 1 (bottom right).

Two robust conclusions follow:

- For all α studied, the true critical field $h_c(\alpha)$ is an order of magnitude larger than $h^\star(\alpha)$; $h^\star$ is therefore decisively *not* a critical point but rather a special ordered-phase point with a particularly clean Néel-cat structure.
- The critical field $h_c(\alpha)$ drifts only mildly with α (increasing from ~ 2.7 to ~ 3.6 over the range $\alpha \in [1.2, 3.0]$), whereas $h^\star(\alpha)$ decreases rapidly.

A more refined finite-size scaling analysis in N would be required to extrapolate $h_c(\alpha)$ to the thermodynamic limit, but the qualitative separation between $h^\star(\alpha)$ and $h_c(\alpha)$ is already clear at $N = 12$.

5 Discussion: rigorous content, numerical evidence and open problems

Mathematically rigorous content

The following statements are fully rigorous and self-contained:

- Lemma 1 gives the exact spectrum and gap of the two-spin block Hamiltonian (3).
- Theorem 1 proves that the Néel cat $|\psi_{\mathrm{cat}}\rangle$ has exactly one bit of entanglement entropy for any dyadic bipartition of a chain of length $N = 2^H$.

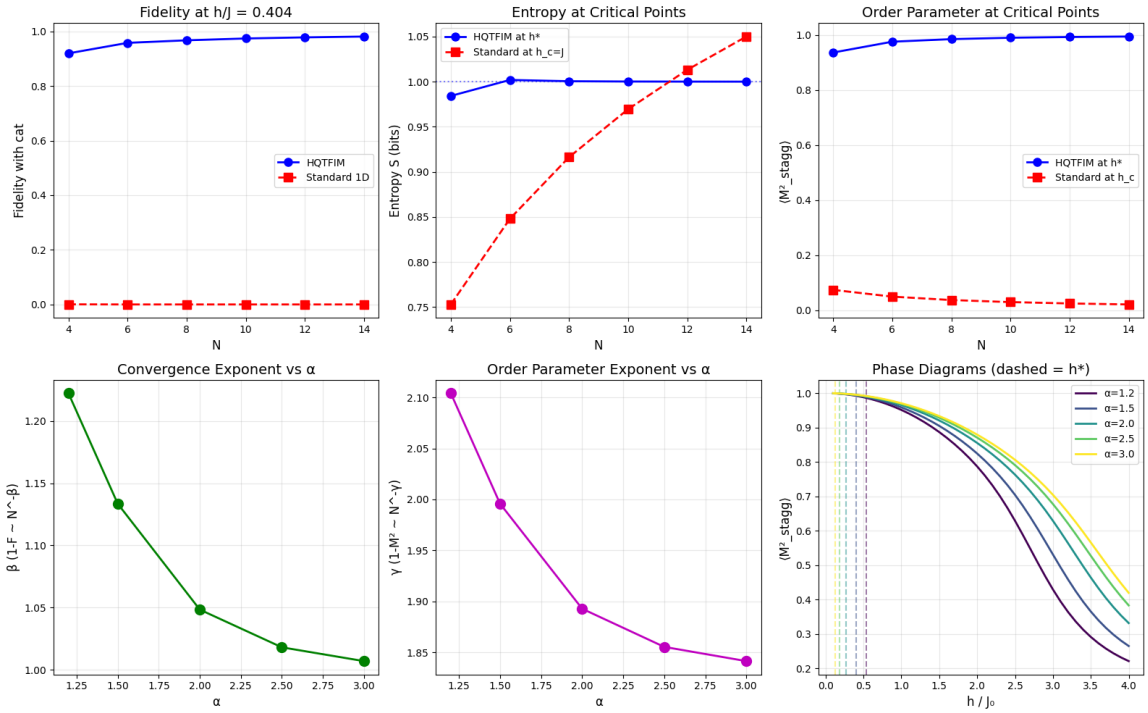

Figure 1: Systematic comparison between the HQTFIM and the standard 1D TFIM. Top left: fidelity of the ground state with the Néel cat at fixed $h/J = 0.404$ for both models. Top middle: entanglement entropy at the critical point of the standard TFIM (h_c^{std}) and at $h^\star$ for the HQTFIM. Top right: staggered order parameter at the same points. Bottom left and middle: exponents $\beta(\alpha)$ and $\gamma(\alpha)$ at $h^\star(\alpha)$. Bottom right: phase diagrams $M^2_{\mathrm{stagg}}(h)$ for several α with dashed lines marking $h^\star(\alpha)$.

- Theorem 2 constructs an explicit TTN representation of $|\psi_{\text{cat}}\rangle$ with bond dimension $\chi = 2$ independent of the system size.
- The numerical tables and plots are obtained by straightforward exact diagonalization followed by explicit evaluation of matrix elements and reduced density matrices; the algorithms are standard and can be verified directly from the supplied code.

Formal RG and phenomenological conclusions

The block RG map of Proposition 1 is exact for a specific formal coarse-graining scheme, but its relation to the rigorous thermodynamic limit of the HQTFIM remains open; in particular, the stability of the low-energy sector under iterated RG steps has not been established analytically. Accordingly, statements involving $h^\star(\alpha)$ as a distinguished field must be regarded as phenomenological rather than fully proved.

Conjecture 1 (Néel-cat ordered point at $h^\star(\alpha)$)**.** *For $\alpha > 1$, at the RG self-similarity field $h = h^\star(\alpha)$ the HQTFIM has long-range Néel order and its even-parity ground state satisfies*

$$\lim_{N\to\infty} F_N = 1, \qquad \lim_{N\to\infty} S_N = 1 \text{ bit}$$

for system sizes $N = 2^H$.

Within this framework, the numerics support the following picture:

- Numerical data are consistent with Conjecture 1. At $h = h^\star(\alpha)$ the HQTFIM appears to be in a Néel-ordered phase, with a ground state that approaches a Néel cat as N increases. This is supported by the increase of F_N, the approach of $M^2_{\text{stagg},N}$ to 1, and the entropy S_N rapidly approaching one bit.
- The rapidly vanishing even–odd splitting Δ_N is naturally interpreted as finite-size tunnelling between symmetry-broken Néel configurations, rather than as a bulk gap closing.
- The power-law corrections $1 - F_N \sim N^{-\beta(\alpha)}$ and $1 - M^2_{\text{stagg},N} \sim N^{-\gamma(\alpha)}$ with $\beta(\alpha) \approx 1$ and $\gamma(\alpha) \approx 2$ indicate algebraic finite-size corrections at $h^\star(\alpha)$, not critical scaling in the sense of a conformal point.
- The true critical field $h_c(\alpha)$ of the HQTFIM is much larger than $h^\star(\alpha)$ and only weakly dependent on α, whereas $h^\star(\alpha)$ decreases strongly with α.

Open problems

Several mathematically sharp questions remain:

- Prove the existence of a Néel-ordered phase for the HQTFIM for $\alpha > 1$ and locate the critical field $h_c(\alpha)$ in the thermodynamic limit, possibly adapting rigorous techniques developed for hierarchical and long-range classical models [Bleher and Sinai, 1975, Bleher and Major, 1988, Bovier, 2006].
- Develop a rigorous multi-scale analysis of the HQTFIM resolvent to control the projection onto the low-energy block subspace at each RG step, in the spirit of Kato perturbation theory [Kato, 1995, Simon, 2015], and derive non-perturbative bounds on $1 - F_N$ as $N \to \infty$.
- Determine the entanglement scaling at the true critical point $h_c(\alpha)$: does the hierarchical geometry modify the universality class of the transition compared to the standard TFIM, and if so, how does the entropy scale with N?
- Characterize the excitation spectrum above the Néel-cat sector at $h^\star(\alpha)$, in particular the scaling of the bulk gap as a function of α and h.

Acknowledgments

The author thanks the quantum information and mathematical physics communities for discussions on hierarchical models, area laws and spectral theory, and acknowledges the availability of open-source scientific Python libraries that made the computations possible.

References

E. Barouch and B. McCoy. Statistical mechanics of the XY model. II. Spin-correlation functions. *Phys. Rev. A*, 3:786–804, 1970.

G. A. Baker Jr. Ising model with a scaling interaction. *Phys. Rev. B*, 5:2622–2633, 1972.

P. M. Bleher and Y. G. Sinai. Investigation of the critical point in models of the type of Dyson's hierarchical models. *Commun. Math. Phys.*, 45:247–278, 1975.

P. M. Bleher and P. Major. Critical phenomena and constructions of Gibbs random fields. *Russ. Math. Surv.*, 43:75–117, 1988.

A. Bovier. *Statistical Mechanics of Disordered Systems*. Cambridge University Press, 2006.

P. Calabrese and J. Cardy. Entanglement entropy and quantum field theory. *J. Stat. Mech.*, P06002, 2004.

P. Calabrese and J. Cardy. Entanglement entropy and conformal field theory. *J. Phys. A*, 42:504005, 2009.

F. J. Dyson. Existence of a phase-transition in a one-dimensional Ising ferromagnet. *Commun. Math. Phys.*, 12:91–107, 1969.

M. B. Hastings. An area law for one-dimensional quantum systems. *J. Stat. Mech.*, P08024, 2007.

T. Kato. *Perturbation Theory for Linear Operators*. Springer, 2nd edition, 1995.

C. Monthus. Random transverse field Ising model on the Dyson hierarchical lattice: solution via a real space RG in configuration space. *J. Stat. Mech.*, 033301, 2018.

P. Pfeuty. The one-dimensional Ising model with a transverse field. *Ann. Phys.*, 57:79–90, 1970.

B. Simon. *Operator Theory*. American Mathematical Society, 2015.

G. Vidal, J. I. Latorre, E. Rico, and A. Kitaev. Entanglement in quantum critical phenomena. *Phys. Rev. Lett.*, 90:227902, 2003.